J Mater Sci (2010) 45:1170–1178
DOI 10.1007/s10853-009-4059-6

Tailoring the tensile/compressive response of magnesium alloy ZK60A using Al_2O_3 nanoparticles

P. Jayaramanavar · M. Paramsothy · A. Balaji · M. Gupta

Received: 13 October 2009 / Accepted: 21 November 2009 / Published online: 9 December 2009

Abstract ZK60A nanocomposites containing Al_2O_3 nanoparticle reinforcement were fabricated using solidification processing followed by hot extrusion and T5 heat treatment. Agglomeration of Al_2O_3 nanoparticles was observed in the nanocomposites. However, in the case of ZK60A/1.0 vol%Al_2O_3 nanocomposite (compared to monolithic ZK60A), increase in tensile strength (up to 14%) without significant decrease in ductility and simultaneous increase in compressive strength (up to 12%) and ductility (+23%) were observed. Here, the strength of ZK60A was increased without significant decrease in ductility. On the other hand, in the case of ZK60A/1.5 vol%Al_2O_3 nanocomposite (compared to monolithic ZK60A), simultaneous increase in tensile strength (up to 6%) and ductility (+26%), but decrease in compressive strength (up to 40%) with increase in ductility (+43%) were observed. Here, the ductility of ZK60A was significantly increased without significant increase in strength. This tailoring of tensile and compressive properties of ZK60A via integration with Al_2O_3 nanoparticles are investigated in this article.

Introduction

Magnesium and aluminum are commonly used light metals in weight-critical structural applications, pertaining to automotive and aerospace industries. Mg is about 35% lighter than Al and both have similar melting points and strengths. Mg is disadvantaged by its limited ductility attributed to its HCP structure, while Al has the advantage of higher ductility given its FCC structure. Also, Mg has a lower elastic modulus (40–45 GPa) than Al (69.6 GPa) [1]. Traditional alloying can be used to increase strength and ductility of Mg [2]. However, many properties of Mg have been improved beyond the limits of alloying with the use of discontinuous reinforcement [3]. In recent years, three methods that have been attempted to improve the strength, ductility, and modulus of Mg are: (a) use of various oxide nanoparticles as well as carbon nanotubes for improving strength and ductility [4–6], (b) use of metallic particles such as Ti and Mo for improving ductility [7–9], and (c) use of micron size ceramic particulates for improving strength and modulus [10, 11]. ZK60A (Mg–Zn–Zr system) is a commonly used Zr-containing (or Al-free) Mg alloy in the world today. It is characterized by: (a) high strength and ductility after aging (T5 heat treatment), (b) good creep resistance, (c) poor arc weldability due to hot-shortness cracking, and (d) excellent resistance weldability. Recently, the superplasticity of the Mg–Zn–Zr system has been studied [12–14]. Here, the superplasticity was attributed to fine grain size (lesser twinning effects) and crystallographic textural effects. Similarly, the superplasticity of Mg–Zn–Zr system reinforced with SiC particles of micron or sub-micron size has been reported [15–17]. Regarding aluminum borate whiskers, the composite interface formed with the Mg–Zn–Zr alloy matrix has also been studied and improved [18]. However, open literature search has revealed that no successful attempt has been made to tailor the tensile and compressive properties of ZK60A with Al_2O_3 or any other nanoparticles, using a high volume production spray-deposition based solidification processing technique.

P. Jayaramanavar
Department of Metallurgical & Materials Engineering, Malaviya National Institute of Technology, Jaipur 302017, India

M. Paramsothy · A. Balaji · M. Gupta (✉)
Department of Mechanical Engineering, National University of Singapore, 9 Engineering Drive 1, Singapore 117576, Singapore
e-mail: mpegm@nus.edu.sg

Accordingly, the primary aim of this study was to tailor the tensile and compressive properties of ZK60A with Al_2O_3 nanoparticles. Disintegrated melt deposition (DMD) [19, 20] followed by hot extrusion was used to synthesize the ZK60A/Al_2O_3 nanocomposites.

Experimental procedures

Materials

In this study, ZK60A (nominally 4.80–6.20 wt%Zn, 0.45 wt%Zr, balance Mg) supplied by Tokyo Magnesium Co. Ltd. (Yokohama, Japan) was used as the matrix material. ZK60A block was sectioned to smaller pieces. All oxide and scale surfaces were removed using machining. All surfaces were washed with ethanol after machining. Al_2O_3 nanoparticles (50 nm size) supplied by Baikowski (Japan) was used as the reinforcement phase.

Primary processing

Monolithic ZK60A was cast using the DMD method [19, 20]. This involved heating ZK60A pieces to 750 °C in an inert Ar gas atmosphere in a graphite crucible using a resistance heating furnace. The crucible was equipped with an arrangement for bottom pouring. Upon reaching the superheat temperature, the melt was stirred for 5 min at 460 rpm using a twin blade (pitch 45°) mild steel impeller to facilitate the uniform distribution of heat. The impeller was coated with Zirtex 25 (86%ZrO_2, 8.8%Y_2O_3, 3.6%SiO_2, 1.2%K_2O and Na_2O, and 0.3% trace inorganics) to avoid iron contamination of the molten metal. The melt was then released through a 10-mm diameter orifice at the base of the crucible. The melt was disintegrated by two jets of argon gas oriented normal to the melt stream and located 265 mm from the melt pouring point. The argon gas flow rate was maintained at 25 lpm. The disintegrated melt was subsequently deposited onto a metallic substrate located 500 mm from the disintegration point. An ingot of 40 mm diameter was obtained following the deposition stage. To form the ZK60A/Al_2O_3 nanocomposites (see Fig. 1), Al_2O_3 nanoparticle powder was placed in alternating layers with ZK60A pieces (having blind holes), with all other DMD parameters unchanged. All deposited ingots were sectioned into billets.

Secondary processing

All billets were machined to 35 mm diameter and hot extruded using 25:1 extrusion ratio on a 150 ton hydraulic press. The extrusion temperature was 350 °C. The billets were held at 400 °C for 60 min in a furnace prior to extrusion. Colloidal graphite was used as a lubricant. Rods of 7 mm were obtained.

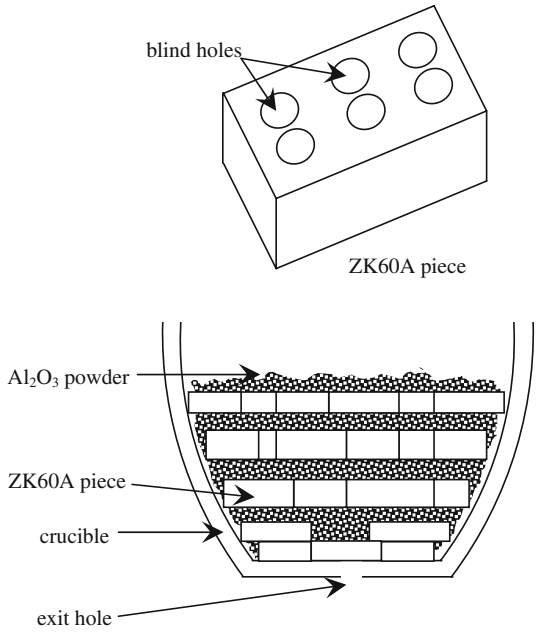

Fig. 1 Arrangement of raw materials in crucible before casting of ZK60A/Al_2O_3 nanocomposites

Heat treatment

T5 heat treatment (aging) was carried out on extruded sections at 150 °C for 1 h using a resistance heating furnace. This selection of temperature and time was made in order to relax the monolithic ZK60A matrix as well as the ZK60A-Al_2O_3 interface of the nanocomposite without recrystallization softening of ZK60A (recrystallization temperature of 99.9+% pure Mg is 150 °C) [21, 22]. Prior to heat treatment, the sections were coated with colloidal graphite and wrapped in aluminum foil to minimize reaction with oxygen present in the furnace atmosphere.

Microstructural characterization

Microstructural characterization studies were conducted on metallographically polished monolithic and nanocomposite extruded samples to determine grain characteristics, as well as nanoparticle reinforcement distribution. Olympus metallographic microscope and Hitachi S4300 Field-Emission Scanning Electron Microscope (FESEM) were used. Image analysis using Scion software was carried out to determine the grain characteristics. X-ray diffraction (XRD) studies were conducted using CuK_α radiation ($\lambda = 1.5406$ Å) with a scan speed of 2°/min in an automated Shimadzu LAB-X XRD-6000 diffractometer to determine the dominant textures in the transverse and longitudinal (extrusion) directions [23–25].

Hardness

Microhardness measurements were made on polished monolithic and nanocomposite extruded samples. Vickers microhardness was measured using Matsuzawa MXT50 automatic digital microhardness tester using 25 gf-indenting load and 15 s dwell time.

Tensile testing

Smooth bar tensile properties of the monolithic and nanocomposite extruded samples were determined based on ASTM E8 M-05. Round tension test samples of 5 mm diameter and 25 mm gauge length were subjected to tension using an MTS 810 machine equipped with an axial extensometer with a strain rate set at 1.67×10^{-4} s^{-1}. Fractography was performed on the tensile fracture surfaces using JEOL JSM-5600LV Scanning Electron Microscope (SEM).

Compressive testing

Compressive properties of the monolithic and nanocomposite extruded samples were determined based on ASTM E9-89a. Samples of 8 mm length (l) and 8 mm diameter (d) where l/d = 1 were subjected to compression using a MTS 810 machine with 0.83×10^{-4} s^{-1} strain rate. Fractography was performed on the compressive fracture surfaces using Hitachi S4300 FESEM.

Results

Macrostructural characteristics

No macropores or shrinkage cavities were observed in the cast monolithic and nanocomposite materials. No macrostructural defects were observed for extruded rods of monolithic and nanocomposite materials.

Microstructural characteristics

Microstructural analysis results revealed no statistically significant change in grain size or aspect ratio of the nanocomposites compared to monolithic material as shown in Table 1 and Fig. 2a. XRD analysis revealed the presence of MgZn phase [26]. Al_2O_3 nanoparticles were observed around Al_2O_3 agglomerates in the nanocomposite as shown in Fig. 2b.

Table 1 Results of grain characteristics and microhardness of ZK60A and ZK60A/Al_2O_3 nanocomposites

Material	Al_2O_3 (vol%)	Grain characteristics[a]		Microhardness (HV)
		Size (μm)	Aspect ratio	
ZK60A	–	14.1 ± 2.4	1.5	97 ± 4
ZK60A/1.0 vol%Al_2O_3	1.00	12.0 ± 2.0	1.5	107 ± 7 (+10)
ZK60A/1.5 vol%Al_2O_3	1.50	15.4 ± 3.1	1.5	92 ± 5 (−5)

Brackets indicate %change with respect to corresponding result of ZK60A

[a] Based on approximately 100 grains

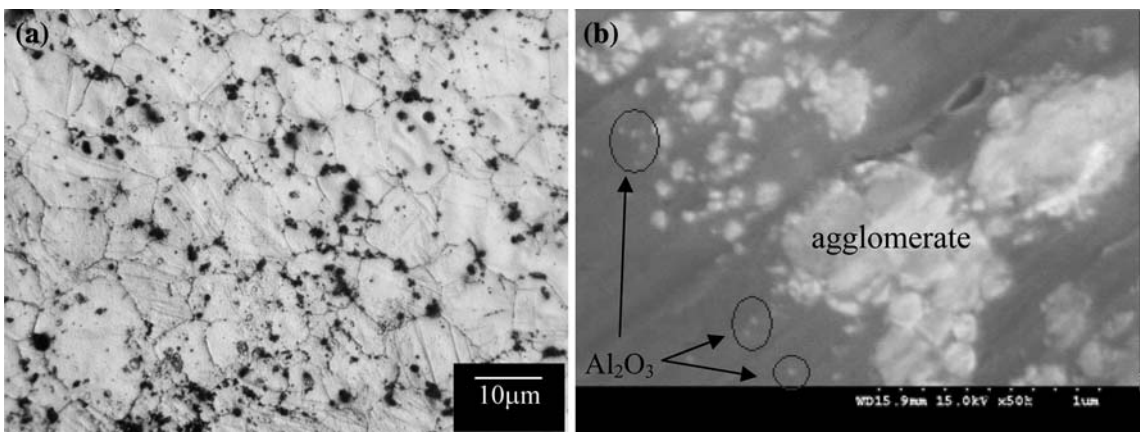

Fig. 2 Representative micrographs showing: **a** grain size in monolithic ZK60A and ZK60A/Al_2O_3 nanocomposites and **b** Al_2O_3 reinforcement distribution (around Al_2O_3 nanoparticle agglomerate) in ZK60A/Al_2O_3 nanocomposites

Table 2 Texture results of ZK60A and ZK60A/Al_2O_3 nanocomposites based on XRD

Material	Section	Plane	Average I/I_{max} [a]
ZK60A	T	1 0 −1 0 prism	0.07
		0 0 0 2 basal	0.26
		1 0 −1 1 pyramidal	**1.00**
	L	1 0 −1 0 prism	0.21
		0 0 0 2 basal	0.48
		1 0 −1 1 pyramidal	**1.00**
ZK60A/1.0 vol%Al_2O_3	T	1 0 −1 0 prism	0.29
		0 0 0 2 basal	0.14
		1 0 −1 1 pyramidal	**1.00**
	L	1 0 −1 0 prism	0.21
		0 0 0 2 basal	0.48
		1 0 −1 1 pyramidal	**1.00**
ZK60A/1.5 vol%Al_2O_3	T	1 0 −1 0 prism	0.24
		0 0 0 2 basal	0.14
		1 0 −1 1 pyramidal	**1.00**
	L	1 0 −1 0 prism	0.23
		0 0 0 2 basal	0.53
		1 0 −1 1 pyramidal	**1.00**

T transverse, *L* longitudinal

[a] I_{max} is XRD maximum intensity from either prism, basal, or pyramidal planes

Bold values indicate dominant textures in T and L sections

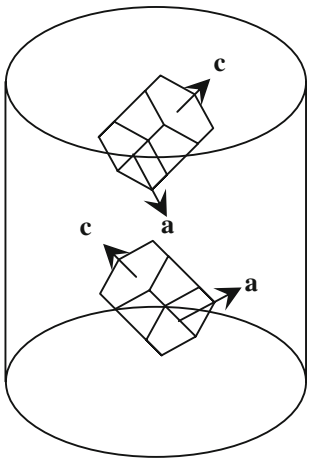

Fig. 3 Schematic diagram showing texture of monolithic ZK60A and ZK60A/Al_2O_3 nanocomposites based on XRD. Vertical axis is parallel to extrusion direction. Each cell is made up of 2 HCP units having 1 common (0 0 0 2) basal plane

Texture results are listed in Table 2 and shown in Fig. 3. In monolithic and nanocomposite materials, the dominant texture in the transverse and longitudinal directions was (1 0 –1 1).

Hardness

The results of microhardness measurements are listed in Table 1. ZK60A/1.0 vol%Al_2O_3 and ZK60A/1.5 vol%Al_2O_3 nanocomposites exhibited higher and lower average hardness than the monolithic material, respectively.

Tensile behavior

The overall results of ambient temperature tensile testing of the extruded materials are shown in Table 3 and Fig. 4a. The strength of ZK60A/1.0 vol%Al_2O_3 was higher compared to monolithic ZK60A, while there was no significant change in failure strain and work of fracture (WOF). The WOF was determined by computing the area under the stress–strain curve. The failure strain and WOF of ZK60A/1.5 vol%Al_2O_3 were higher compared to monolithic ZK60A, while there was no significant change in strength. The fractured surface of all extruded materials exhibited mixed (ductile + brittle) mode of fracture as shown in Fig. 5a, b.

Compressive behavior

The overall results of ambient temperature compressive testing of the extruded materials are shown in Table 4 and Fig. 4b. The strength at all strain levels, failure strain, and WOF of ZK60A/1.0 vol%Al_2O_3 were higher compared to monolithic ZK60A. The strength at all strain levels of ZK60A/1.5 vol%Al_2O_3 was lower compared to monolithic ZK60A while the failure strain and WOF were higher. The fractured surface of monolithic ZK60A appeared smooth while that of ZK60A/Al_2O_3 nanocomposites appeared slightly rough as shown in Fig. 5c, d.

Table 3 Results of tensile testing of ZK60A and ZK60A/Al_2O_3 nanocomposites

Material	0.2%TYS (MPa)	UTS (MPa)	Failure strain/elongation (%)	WOF (MJ/m^3)[a]
ZK60A	139 ± 4	246 ± 4	20.2 ± 2.0	46 ± 4
ZK60A/1.0 vol%Al_2O_3	158 ± 4 (+14)	266 ± 7 (+8)	19.4 ± 2.0 (−4)	49 ± 5 (+7)
ZK60A/1.5 vol%Al_2O_3	147 ± 8 (+6)	252 ± 5 (+2)	25.5 ± 1.0 (+26)	61 ± 2 (+33)
As-fabricated magnesium microcomposites for comparison:				
AZ91 [45]	155	195	4.8	–
AZ91/20.0 vol%Al_2O_3 [45]	230 (+48)	295 (+51)	1.5 (−69)	–
Mg [10]	100 ± 4	258 ± 16	7.7 ± 1.2	–
Mg/3.2 vol%Ni [10]	370 ± 12 (+270)	389 ± 5 (+51)	3.1 ± 0.1 (−60)	–
Mg [33]	97 ± 2	173 ± 1	7.4 ± 0.2	11.1 ± 0.3
Mg/1.1vol% Al_2O_3 [33]	209 ± 1 (+115)	242 ± 3 (+40)	3.5 ± 0.3 (−53)	7.0 ± 0.9 (−37)
Heat treated magnesium microcomposites for comparison:				
Mg [26]	69–105	165–205	5–8	–
Mg/6.5 vol%SiC [22]	130 ± 12 (+24)	191 ± 11 (−7)	12.8 ± 1.53 (+60)	–
AZ91 T6 [46]	263 ± 12	358 ± 5	7 ± 4	–
AZ91/3.59 vol%Cu T6 [46]	299 ± 5 (+14)	382 ± 6 (+7)	6 ± 1 (−14)	–

Brackets indicate %change with respect to corresponding result of monolithic material

[a] Obtained from engineering stress–strain diagram using EXCEL software

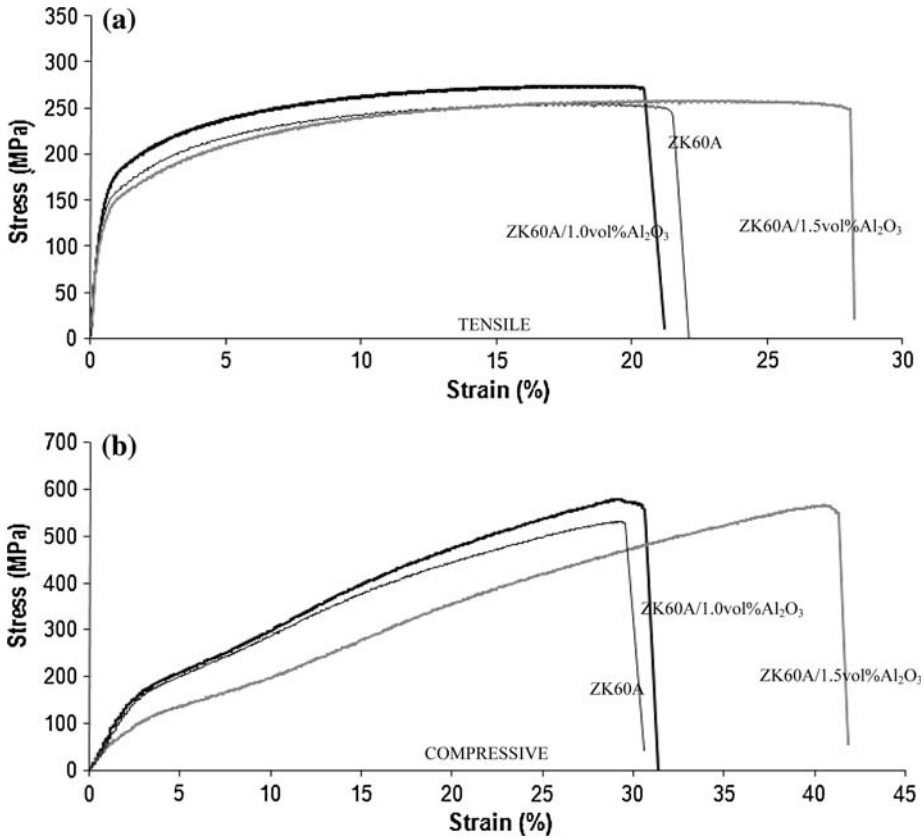

Fig. 4 Representative: **a** tensile and **b** compressive stress–strain curves of monolithic ZK60A and ZK60A/Al_2O_3 nanocomposites

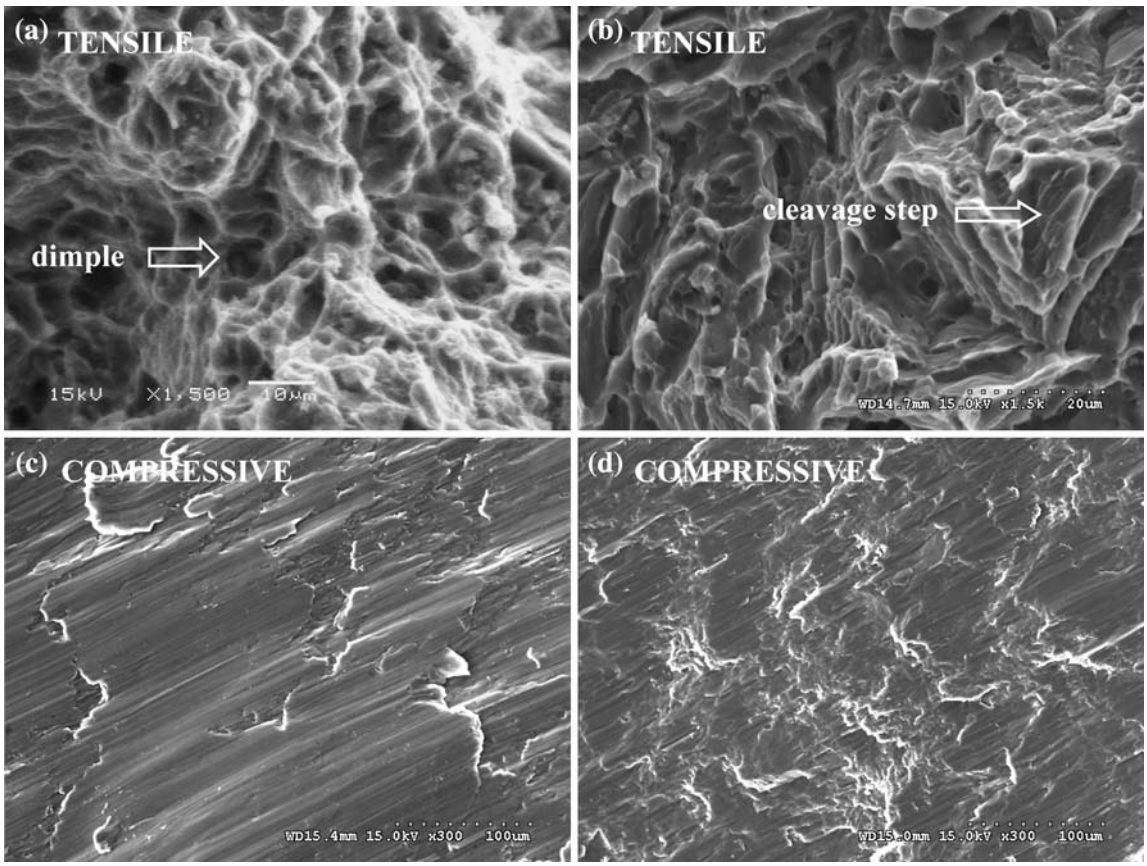

Fig. 5 Representative tensile fractographs of: **a** monolithic ZK60A and ZK60A/1.0 vol%Al_2O_3 nanocomposite and **b** ZK60A/1.5 vol%Al_2O_3 nanocomposite. Representative compressive fractographs of: **c** monolithic ZK60A and **d** ZK60A/Al_2O_3 nanocomposites

Table 4 Results of compressive testing of ZK60A and ZK60A/Al_2O_3 nanocomposites

Material	0.2%CYS (MPa)	UCS (MPa)	Failure strain (%)	WOF (MJ/m^3)[a]
ZK60A	136 ± 11	538 ± 14	19.6 ± 1.8	96 ± 6
ZK60A/1.0 vol%Al_2O_3	152 ± 5 (+12)	577 ± 8 (+7)	24.2 ± 1.5 (+23)	118 ± 5 (+22)
ZK60A/1.5 vol%Al_2O_3	82 ± 9 (-40)	565 ± 10 (+5)	28.1 ± 2.9 (+43)	136 ± 16 (+42)
As-fabricated magnesium microcomposites for comparison:				
RZ5[b] [47]	–	308	16.7	–
RZ5/22.0 vol%Saffil[c] [47]	–	445 (+44)	5.2 (–69)	–

Brackets indicate %change with respect to corresponding result of monolithic material

[a] Obtained from engineering stress–strain diagram using EXCEL software

[b] RZ5 has nominal composition of 4.2 wt%Zn, 0.35 wt%Zr, 1.3 wt%RE (rare earth metals), balance Mg

[c] Saffil (ICI tradename) has nominal dimensions of 3 μm diameter and 150 μm length, and approximate composition of 5 wt%silica and balance δ-alumina

Discussion

Synthesis of monolithic ZK60A and ZK60A/Al_2O_3 nanocomposites

Synthesis of monolithic and nanocomposite materials, the final form being extruded rods, was successfully accomplished with: (a) no detectable metal oxidation and (b) no detectable reaction between graphite crucible and melts. The inert atmosphere used during DMD was effective in preventing oxidation of the Mg melt. No stable carbides of Mg formed due to reaction with graphite crucible.

Microstructural characteristics

Microstructural characterization of extruded samples is discussed in terms of: (a) grain characteristics and (b) Al_2O_3 nanoparticle reinforcement distribution.

Nearly equiaxed grains were observed in monolithic material and nanocomposite as shown in Table 1 and Fig. 2a. Change in grain size of the nanocomposites compared to monolithic material was statistically insignificant, suggesting the inability of Al_2O_3 nanoparticles to effectively serve as either nucleation sites or obstacles to grain growth during solid state cooling.

The agglomeration of Al_2O_3 nanoparticles as shown in Fig. 2b can be attributed to: (a) leaching of Zn and Zr alloying elements from the ZK60A matrix [27] and (b) reaction of the Mg matrix with Al_2O_3 nanoparticles [27, 28]. Regarding (a), Energy Dispersive X-Ray Spectroscopy (EDS) revealed the presence of Zn and Zr in the Al_2O_3 nanoparticle agglomerate. Regarding (b), XRD indicated the presence of MgO formed due to reaction between Mg and Al_2O_3 [27, 28]. The reasonably uniform distribution of Al_2O_3 nanoparticles around the Al_2O_3 nanoparticle agglomerate can be attributed to: (a) minimal gravity-associated segregation due to judicious selection of stirring parameters [19], (b) good wetting of Al_2O_3 nanoparticles by the alloy matrix [29–31], (c) argon gas disintegration of metallic stream [32], and (d) dynamic deposition of composite slurry on substrate followed by hot extrusion.

Mechanical behavior

Hardness

An increase in microhardness by 10% was observed in ZK60A/1.0 vol%Al_2O_3 compared to monolithic material as listed in Table 1. This was consistent with earlier observations made on Mg/Al_2O_3, AZ31/C_{60}, and AZ31/MWCNT nanocomposites [5, 33, 34] despite leaching of Zn and Zr alloying elements from the ZK60A matrix [27]. The increase in hardness of ZK60A/1.0 vol%Al_2O_3 can be attributed to: (a) Al_2O_3 nanoparticle agglomerates in the matrix, (b) reasonably uniform distribution of Al_2O_3 nanoparticles (around the Al_2O_3 nanoparticle agglomerates) in the matrix, (c) MgO formed due to reaction between Mg and Al_2O_3 [27, 28], and (d) higher constraint to localized matrix deformation during indentation due to the presence of (a)–(c) [5, 6, 33].

In the case of ZK60A/1.5 vol%Al_2O_3, no statistically significant change in hardness was exhibited compared to monolithic material. This was despite (a)–(d) and can be attributed to leaching of Zn and Zr alloying elements from the ZK60A matrix [27] to a greater extent compared to ZK60A/1.0 vol%Al_2O_3.

Tensile and compressive behavior

Strength The tensile and compressive strengths of monolithic material and nanocomposites are listed in Tables 3 and 4 (and shown in Fig. 4a, b), respectively. 0.2%TYS and UTS were enhanced by 14% and 8%, respectively, in ZK60A/1.0 vol%Al_2O_3 compared to monolithic material. In comparison of compressive strength, 0.2%CYS and UCS of ZK60A/1.0 vol%Al_2O_3 were enhanced by 12% and 7%, respectively, compared to monolithic material. The compressive stress detected at any given strain was higher for ZK60A/1.0 vol%Al_2O_3 compared to monolithic material as shown in Fig. 4b. The tensile/compressive strength increase of ZK60A/1.0 vol%Al_2O_3 compared to monolithic material was despite: (a) Al_2O_3 nanoparticle agglomeration (see Fig. 2b) and (b) leaching of Zn and Zr alloying elements from the ZK60A matrix [27]. This tensile/compressive strength increase can be attributed to well known factors (pertaining to reinforcement) such as: (a) dislocation generation due to elastic modulus mismatch and coefficient of thermal expansion mismatch between the matrix and reinforcement [5, 6, 35, 36], (b) Orowan strengthening mechanism [35–37], and (c) load transfer from matrix to reinforcement [5, 35].

In the case of ZK60A/1.5 vol%Al_2O_3, 0.2%TYS and UTS were enhanced by 6% and 2%, respectively, compared to monolithic material. This was similar to the ZK60A/1.0 vol%Al_2O_3 case. However, in comparison of compressive strength, 0.2%CYS and UCS of ZK60A/1.5 vol%Al_2O_3 were decreased and enhanced by 40% and 5%, respectively, compared to monolithic material. The compressive stress detected at much of the given strain was significantly lower for ZK60A/1.5 vol%Al_2O_3 compared to monolithic material as shown in Fig. 4b. This can be attributed to: (a) Al_2O_3 nanoparticle agglomeration and (b) leaching of Zn and Zr alloying elements from the ZK60A matrix [27], each to a greater extent compared to ZK60A/1.0 vol%Al_2O_3.

In both monolithic ZK60A and ZK60A/1.0 vol%Al_2O_3, 0.2%TYS was about 1.0 times the 0.2%CYS. Here, tensile/compressive yield stress isotropy was present despite half the strain rate used (less strain hardening) in compressive testing compared to tensile testing. This can be attributed to $\{1\,0\,1\,-2\}\,\langle 1\,0\,1\,-1\rangle$-type twinning being activated along the *c*-axis of the HCP unit cell in Fig. 3 (see Table 2 also) with comparatively similar ease in both tension and compression along the *c*-axis, based on the 45° angle between the *c*-axis and the vertical axis [38, 39]. In the case of ZK60A/1.5 vol%Al_2O_3, 0.2%TYS was about 1.8 times the 0.2%CYS despite the similarity in crystallographic texture compared to monolithic ZK60A and ZK60A/1.0 vol%Al_2O_3. Here, the significant tensile/compressive yield stress anisotropy can be attributed to Al_2O_3

nanoparticle agglomeration to a greater extent compared to ZK60A/1.0 vol%Al_2O_3.

Failure strain The tensile and compressive failure strains of monolithic material and nanocomposite are listed in Tables 3 and 4 (and based on stress–strain curves shown in Fig. 4a, b), respectively. Compared to monolithic material, tensile failure strain was slightly decreased by 4% in ZK60A/1.0 vol%Al_2O_3. Compared to monolithic material, compressive failure strain was enhanced by 23% in ZK60A/1.0 vol%Al_2O_3. In the case of ZK60A/1.5 vol%Al_2O_3, tensile and compressive failure strains were enhanced by 26% and 43%, respectively, compared to monolithic material. This was despite: (a) Al_2O_3 nanoparticle agglomeration (see Fig. 2b) and (b) leaching of Zn and Zr alloying elements from the ZK60A matrix [27]. The tensile/compressive failure strain increases in ZK60A/Al_2O_3 nanocomposites compared to monolithic material can be attributed to the following factors (pertaining to reinforcement): (a) presence and reasonably uniform distribution of Al_2O_3 nanoparticles (around the Al_2O_3 nanoparticle agglomerates) [33, 40] and (b) overall ZK60A–Al_2O_3 matrix–particle interfacial relaxation [21, 22]. In the case of reasonably uniform distribution of ceramic nanoparticles, it has been shown in previous studies that ceramic nanoparticles provide sites where cleavage cracks are opened ahead of the advancing crack front. This: (1) dissipates the stress concentration which would otherwise exist at the crack front and (2) alters the local effective stress state from plane strain to plane stress in the neighborhood of crack tip [33, 40]. In the case of overall matrix–particle interfacial relaxation, it has been shown in previous studies that reducing the stress built up at the matrix–particle interface leads to enhanced ductility [21, 22]. The significantly higher increments in tensile and compressive failure strains of ZK60A/1.5 vol%Al_2O_3 (+26% and +43%, respectively) compared to ZK60A/1.0 vol%Al_2O_3 (−4% and +23%, respectively) can be attributed to factors (a) and (b) each occurring to a greater extent in ZK60A/1.5 vol%Al_2O_3.

Tensile fracture behavior of both monolithic material and nanocomposites was mixed (ductile + brittle) as shown in Fig. 5a, b. However, the tensile fractured surface of ZK60A/1.5 vol%Al_2O_3 had higher occurrence of larger cleavage steps compared to that of ZK60A/1.0 vol%Al_2O_3 and monolithic material. This can be attributed to greater extent of (a) Al_2O_3 nanoparticle agglomeration and (b) leaching of Zn and Zr alloying elements from the ZK60A matrix [27] in ZK60A/1.5 vol%Al_2O_3. The involvement of shear and formation of dimples during deformation and fracture can be attributed to shear localization around: (a) intermetallic particles and (b) voids in the deformed matrix surrounding the intermetallic particles, in alloys [41, 42]. The greater extent of leaching of Zn and Zr alloying elements from the ZK60A matrix [27] in ZK60A/1.5 vol%Al_2O_3 lead to a reduction in intermetallic particle content in the ZK60A matrix. This in turn reduced the involvement of shear and formation of dimples during deformation and fracture of ZK60A/1.5 vol%Al_2O_3. Cleavage fracture for relatively ductile pure magnesium has been previously reported [43]. Compressive fracture behavior of ZK60A/Al_2O_3 nanocomposites was relatively less ductile (slightly rough fracture surface exhibited) compared to monolithic material as shown in Fig. 5c, d. The slightly rough fracture surface exhibited by the ZK60A/Al_2O_3 nanocomposites can be attributed to the Al_2O_3 nanoparticle agglomeration in the ZK60A matrix.

Work of fracture The tensile and compressive WOF of monolithic material and nanocomposites are listed in Tables 3 and 4 (and illustrated in Fig. 4a, b), respectively. WOF quantified the ability of the material to absorb energy up to fracture under load [44]. Compared to monolithic material, tensile WOF and compressive WOF were enhanced by 7% and 22%, respectively, in ZK60A/1.0 vol%Al_2O_3. Compared to monolithic material, tensile WOF and compressive WOF were enhanced further by 33% and 42%, respectively, in ZK60A/1.5 vol%Al_2O_3.

The tensile and compressive properties of magnesium microcomposites are listed in Tables 3 and 4, respectively, for comparison purposes. The compressive data of magnesium microcomposites available from research literature are limited. In all cases of as-fabricated microcomposites, the strength was significantly increased (up to 270%) while the ductility was significantly decreased (up to 69%), compared to monolithic material. However, regarding heat treated microcomposites in tension, neither the strength nor the ductility was significantly decreased compared to monolithic material. Here, up to 24% increase in strength and more importantly up to 60% significant increase in ductility was simultaneously observed as in the case of heat treated Mg/6.5 vol%SiC microcomposite compared to monolithic Mg. This indicated the comparable benefit in tensile properties of magnesium microcomposites that can be gained with the use of suitable heat treatment.

Overall and comparing both ZK60A/Al_2O_3 nanocomposites, the higher strength exhibited by ZK60A/1.0 vol%Al_2O_3 shows its potential to be used in strength critical design, while the significantly higher increment in WOF exhibited by ZK60A/1.5 vol%Al_2O_3 shows its potential to be used in damage tolerant design.

Conclusions

1. Monolithic ZK60A and ZK60A/Al_2O_3 nanocomposites can be successfully synthesized using the DMD

technique followed by hot extrusion and T5 heat treatment (aging).

2. Compared to monolithic ZK60A, strength was enhanced more in ZK60A/1.0 vol%Al_2O_3 than in ZK60A/1.5 vol%Al_2O_3. This can be attributed to: (a) Al_2O_3 nanoparticle agglomeration and (b) leaching of Zn and Zr alloying elements from the ZK60A matrix, each to a greater extent in ZK60A/1.5 vol%Al_2O_3.
3. Compared to monolithic ZK60A, failure strain was enhanced more in ZK60A/1.5 vol%Al_2O_3 than in ZK60A/1.0 vol%Al_2O_3. This can be attributed to: (a) presence and reasonably uniform distribution of Al_2O_3 nanoparticles (around the Al_2O_3 nanoparticle agglomerates) and (b) overall ZK60A–Al_2O_3 matrix–particle interfacial relaxation, each occurring to a greater extent in ZK60A/1.5 vol%Al_2O_3.
4. Compared to monolithic ZK60A, WOF was enhanced further in ZK60A/1.5 vol%Al_2O_3 than in ZK60A/1.0 vol%Al_2O_3.

Acknowledgements M. Paramsothy is the principle author of this article and acknowledges A. Balaji for microstructural and tensile characterization, and P. Jayaramanavar for compressive characterization. K.S. Tun and Q.B. Nguyen are acknowledged for their kind assistance in processing and characterization.

References

1. Clyne TW, Withers PJ (1993) An introduction to metal matrix composites. Cambridge University Press, Cambridge
2. Brandes EA, Brook GB (eds) (1998) Smithells light metals handbook. Reed Educational and Professional Publishing Ltd, USA, p 40
3. Ferkel H, Mordike BL (2001) Mater Sci Eng A 298:193
4. Hassan SF, Gupta M (2006) Compos Struct 72:19
5. Hassan SF, Gupta M (2006) J Mater Sci 41:2229. doi:10.1007/s10853-006-7178-3
6. Goh CS, Wei J, Lee LC, Gupta M (2006) Nanotechnology 17:7
7. Hassan SF, Gupta M (2002) J Alloys Compd 345:246
8. Perez P, Garces G, Adeva P (2004) Compos Sci Technol 64:145
9. Wong WLE, Gupta M (2005) Adv Eng Mater 7:250
10. Hassan SF, Gupta M (2002) J Alloys Compd 335:L10
11. Huard G, Angers R, Krishnadev MR, Tremblay R, Dube D (1999) Can Metall Q 38:193
12. Lapovok R, Thomson PF, Cottam R, Estrin Y (2005) Mater Sci Eng A 410–411:390
13. Kim WJ, Kim MJ, Wang JY (2009) Mater Sci Eng A. doi:10.1016/j.msea.2009.08.064
14. Watanabe H, Mukai T, Higashi K (1999) Scripta Mater 40(4):477
15. Nieh TG, Schwartz AJ, Wadsworth J (1996) Mater Sci Eng A 208:30
16. Yan F, Wu K, Wu GL, Lee BL, Zhao M (2003) Mater Lett 57:1992
17. Feng Y, Zhou X, Min Z, Kun W (2005) Scripta Mater 53:361
18. Sasaki G, Wang WG, Hasegawa Y, Choi YB, Fuyama N, Matsugi K, Yanagisawa O (2007) J Mater Proc Technol 187–188:429
19. Tham LM, Gupta M, Cheng L (1999) Mater Sci Technol 15:1139
20. Gupta M, Lai MO, Lim SC (1997) J Alloys Compd 260:250
21. Ugandhar S, Gupta M, Sinha SK (2006) Compos Struct 72:266
22. Lim SCV, Gupta M (2006) Mater Sci Technol 19:803
23. Paramsothy M, Srikanth N, Hassan SF, Gupta M (2008) Mater Sci Eng A 494:436
24. Paramsothy M, Hassan SF, Srikanth N, Gupta M (2008) J Phys D 41:175402
25. Paramsothy M, Hassan SF, Srikanth N, Gupta M (2009) J Alloys Compd 482:73
26. Avedesian MM, Baker H (1999) ASM specialty handbook: magnesium and magnesium alloys. ASM International®, Ohio, p 10, 40
27. Evans JT (1986) Acta Metall 34(10):2075
28. Guden M, Akil O, Tasdemirci A, Ciftcioglu M, Hall IW (2006) Mater Sci Eng A 425:145
29. Han BQ, Dunand DC (2000) Mater Sci Eng A 277:297
30. Eustathopoulos N, Nicholas MG, Drevet B (1999) Wettability at high temperatures, vol 3. Pergamon Materials Series, Pergamon, New York
31. Gilchrist JD (1989) Extraction metallurgy, vol 3. Pergamon Press, New York
32. Gupta M, Lai MO, Soo CY (1996) Mater Sci Eng A 210:114
33. Hassan SF, Gupta M (2006) J Alloys Compd 419:84
34. Hassan SF, Gupta M (2005) Metall Mater Trans A 36(8):2253
35. Szaraz Z, Trojanova Z, Cabbibo M, Evangelista E (2007) Mater Sci Eng A 462:225
36. Dai LH, Ling Z, Bai YL (2001) Compos Sci Technol 61:1057
37. Hull D, Bacon DJ (2002) Introduction to dislocations, 4th edn. Butterworth-Heinemann, Oxford, p 43, 231
38. Laser T, Hartig C, Nurnberg MR, Letzig D, Bormann R (2008) Acta Mater 56:2791
39. Bohlen J, Yi SB, Swiostek J, Letzig D, Brokmeier HG, Kainer KU (2005) Scripta Mater 53:259
40. Hassan SF, Gupta M (2007) J Alloys Compd 429:176
41. Spencer K, Corbin SF, Lloyd DJ (2002) Mater Sci Eng A 325:394
42. Hu XH, Jain M, Wilkinson DS, Mishra RK (2008) Acta Mater 56:3187. doi:10.1016/j.actamat.2008.02.048
43. Paramsothy M, Srikanth N, Gupta M (2008) J Alloys Compd 461:200
44. Reed-Hill RE (1964) Physical metallurgy principles, 2nd edn. D Van Nostrand Company, New York, p 192 267, 725
45. Purazrang K, Abachi P, Kainer KU (1994) Composites 25(4): 296
46. Ho KF, Gupta M, Srivatsan TS (2004) Mater Sci Eng A 369: 302
47. Towle DJ, Friend CM (1993) Mater Sci Technol 9:35